JOURNAL OF MATERIALS SCIENCE 35 (2000) 3615–3629

Comparative performance of selected bond coats in advanced thermal barrier coating systems

H. M. TAWANCY, N. SRIDHAR, N. M. ABBAS
Materials Characterization Laboratory, Metrology, Standards, and Materials Division, Research Institute, King Fahd University of Petroleum and Minerals

D. S. RICKERBY
P.O. Box 1639, Dhahran 31261, Saudi Arabia, Rolls-Royce plc, Derby, UK

An investigation was carried out to determine the comparative performance of selected bond coats representing the diffusion aluminides and overlays in thermal barrier coating systems. Emphasis was placed upon oxidation behavior, thermal stability, and failure mechanism. Isothermal oxidation tests were carried out at temperatures in the range of 1000 °C to 1150 °C. Scanning electron microscopy combined with energy dispersive x-ray spectroscopy, x-ray diffraction, and transmission electron microscopy were used to characterize the coating microstructure. Among the bond coats examined, overlays exhibited the best performance followed by Pt-aluminides and simple alunimides for a given alloy substrate. However, for all types of bond coats, failure of the coating system occurred by decohesion of the oxide scale at the oxide-bond coat interface. All bond coats examined were found to be degraded by oxidation and interdiffusion with the alloy substrate permitting the formation of non-protective oxide scale near the bond coat surface. Platinum as well as active elements such as Hf and Y were identified as key elements in improving the performance of thermal barrier coating systems.

1. Introduction

Increasing turbine entry temperature (TET) is considered the dominant factor in new designs of large turbofan engines, e.g. [1]. Improved cooling methods and use of thermal barrier coatings are considered to be the most technically and economically feasible means for increasing the operating temperature of a gas turbine engine [2]. Design concepts of aero-engines require that turbine blades must maintain both mechanical strength and surface integrity over thousands of hours at elevated temperatures under the combined effect of high stress levels and very corrosive environment. With continued demand for higher strength, newer alloys and manufacturing techniques have been developed. Inevitably, however, there has been a steady decrease in environmental resistance limiting component life and requiring the application of surface protection systems. An aluminizing treatment has been the earliest coating method involving diffusion of aluminum into the surface layers of superalloy substrate. Upon exposure to elevated temperatures, the Al-rich surface layer develops a slow growing and thermodynamically stable film of Al_2O_3 acting as an effective barrier between the alloy and environment, e.g. [3]. With the increasing importance of surface degradation as a component life-limiting factor, more advanced coating systems based upon the above concept have been developed.

An increase in turbine entry temperature by as much as 50–100 °C equivalent to 2–4 generations of superalloy development can be achieved by means of a thermal barrier coating system (TBC) where a conventional metallic coating (diffusion aluminide or overlay) is insulated by a ceramic coat usually ZrO_2 stabilized by the addition of about 8% Y_2O_3 [4, 5]. Prior to depositing the ceramic top coat, the metallic bond coat is made to develop a thin layer of Al_2O_3 scale about 1 μm in thickness to act as a glue bonding the top coat to the bond coat and provide additional oxidation resistance. In addition to reducing the temperature difference between the outer surfaces of the top coat and bond coat by as much as 150 °C, these coating systems reduce thermal shock loads on the blades [4].

Thermal barrier coating systems have been successfully used on stationary components such as vane platforms [6–8], and a considerable effort is now directed toward extending their application to turbine blades. This is largely dependent upon the use of suitable bond coat systems. Earlier studies have demonstrated that TBC systems fail be decohesion between the oxide layer developed by the bond coat and the top ceramic coat, e.g. [9–16]. It is the objective of this paper to examine the comparative oxidation characteristics of various bond coat systems including aluminide, platinum

TABLE I Nominal chemical composition of alloy substrates (weight percent)

Element	MAR-M 002DS	SRR 99	RR 2000
Ni	Balance	Balance	Balance
Co	10	5	15
Cr	9	8.5	10
Al	5.5	5.5	5.5
Ti	1.5	2.2	4
Hf	1.25	0.05[a]	0.05[a]
W	10	9.5	0.5[a]
Mo	0.5[a]	0.5[a]	3
Ta	2.5	2.8	0.05[a]
Zr	0.055	0.01[a]	0.01[a]
V	—	—	1
Fe	0.5[a]	0.1[a]	0.1[a]
B	0.015	—	
C	0.15	0.015	0.015 [a]

[a]Maximum.

aluminides and overlays with particular emphasis on their thermal stability.

2. Experimental procedure

Alloy substrates included in this study were the directionally solidified alloy MAR M 002 DS* and the single-crystal alloys SRR 99* and RR 2000 (*MAR M is a registered trademark of Martin Marietta Corp., SRR and RR are registered trademark of Rolls-Royce plc). Their nominal compositions are listed in Table I. Simple aluminide coatings (nominal Al content = 25 weight %) were applied on rod samples (8 mm in diameter) of the alloy substrate by the pack cementation process [8, 17]. Platinum aluminizing to produce nominal Pt and Al contents of 55 weight % and 25 weight % respectively was performed by first electroplating a 6–8 mm thick layer of Pt on the alloy surface followed by diffusion and aluminizing treatments [18]. Both aluminide and Pt-aluminide coatings had a nominal thickness of 50 μm in the solution-annealed condition. An overlay coating of the MCrAlY-type with a nominal composition (weight %) of Co, 32Ni, 21Cr, 8Al, 0.5Y was applied by the standard technique of vacuum plasma spraying [4, 19]. In the heat-treated condition; the nominal coating thickness was about 100 μm. A 250 μm layer of the ceramic top coat (ZrO_2-8 weight % Y_2O_3) was applied by the electron beam vacuum evaporation technique Oxidation tests were carried out at 1100 °C and 1150 °C with a 24-hour cycling period to room temperature. Scanning electron microscopy combined with energy dispersive x-ray spectroscopy, x-ray diffraction, and transmission electron microscopy were used to characterize the coating microstructure.

3. Results and discussion

3.1. Comparative life of coating system at 1150 °C

A typical microstructure of a cross-section of a thermal barrier coating system (TBC) is shown in Fig. 1. Initially, the interfacial oxide layer of Al_2O_3 base scale acting as a glue between the top coat and bond coat

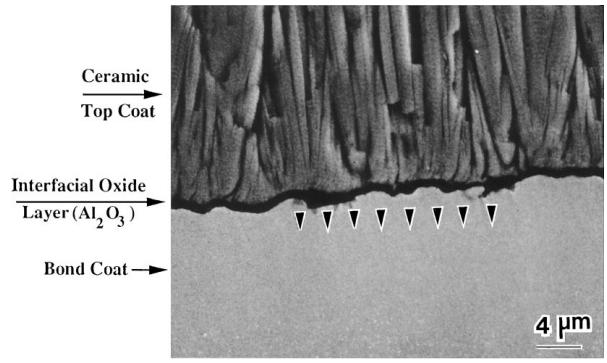

Figure 1 A typical microstructure of a cross-section of a thermal barrier coating system in the heat-treated condition; the arrows indicate the growth mode of the oxide during exposure at elevated temperatures.

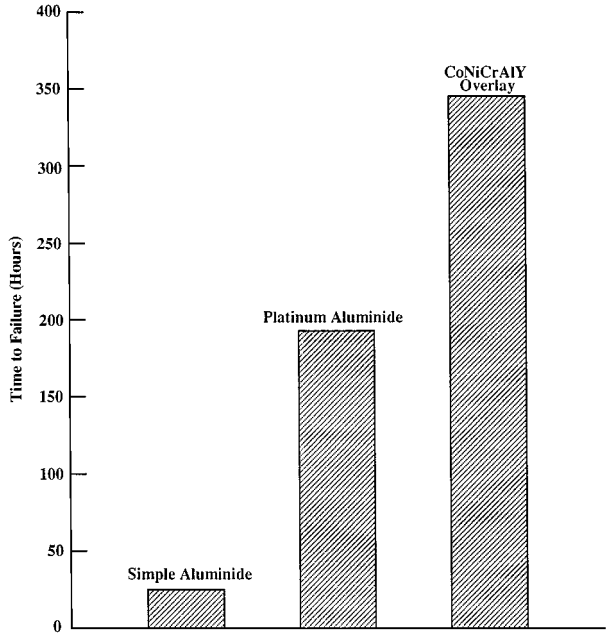

Figure 2 Comparative average life of various bond coats as determined from oxidation tests in air at 1150 °C with a 24-hour cyclic period to room temperature (alloy MAR M 002 DS substrate).

has a thickness of about 1 μm. To distinguish the oxide developed during subsequent exposure at elevated temperatures, it is usually referred to as thermally grown oxide. Consistent with the results of earlier studies [17], the thermally grown oxide was found to develop by inward diffusion of oxygen, i.e. oxide growth occurred by inward movement of the oxide-bond coat interface as shown in Fig. 1. This was indicated by the absence of oxides of substrate elements near the oxide-top coat interface as shown later.

As an example, Fig. 2 illustrates the average life of the TBC system for various types of bond coats on alloy MAR M 002DS as determined from oxidation tests in air at 1150 °C with a 24-hour cyclic period to room temperature. It is demonstrated later that the failure mode for all bond coats examined was decohesion between the thermally grown oxide and bond coat. Spallation of the top coat occurred only during cooling and as room temperature was approached indicating that thermal stresses provided the driving force for decohesion between the oxide and bond coat.

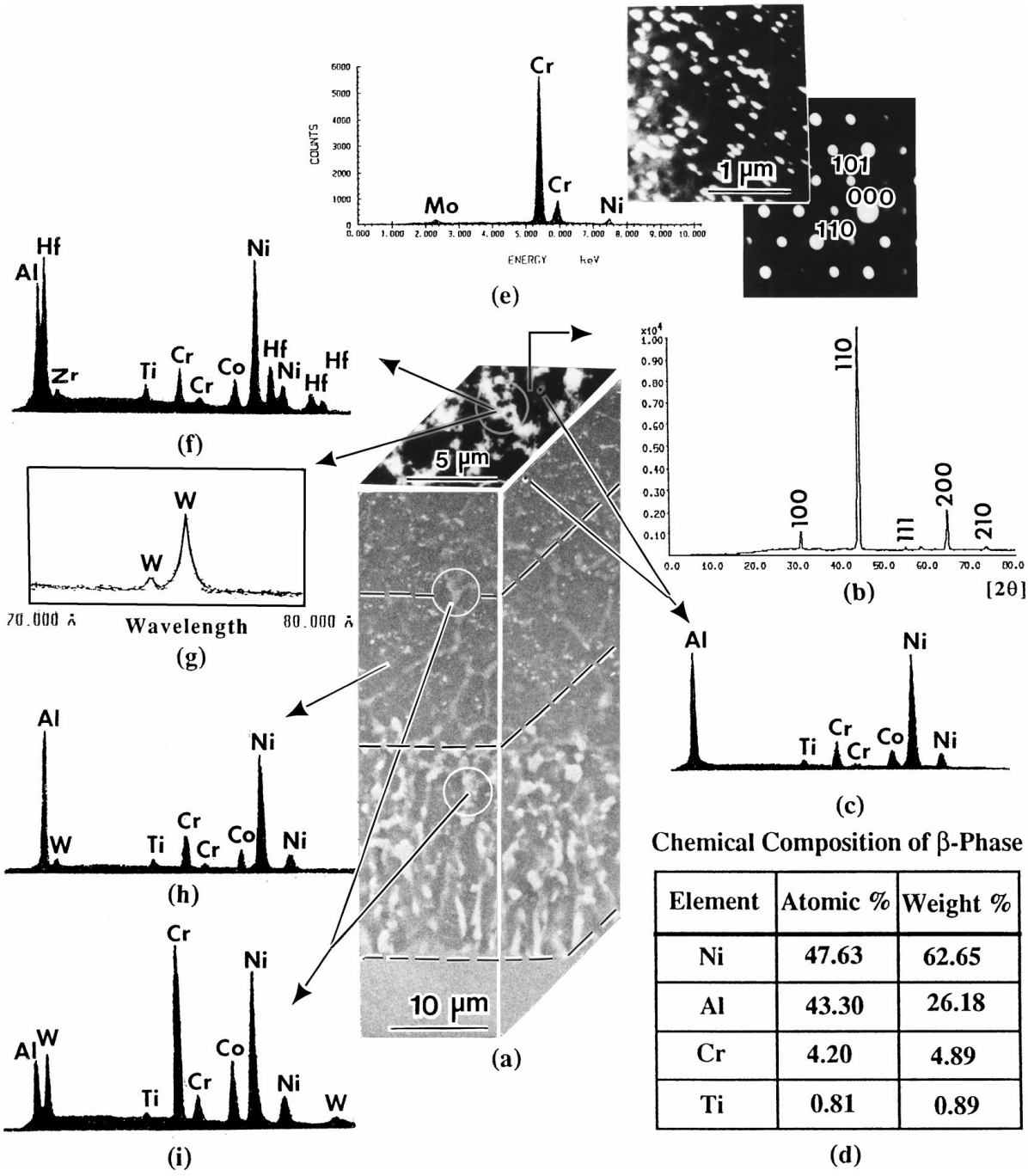

Chemical Composition of β-Phase

Element	Atomic %	Weight %
Ni	47.63	62.65
Al	43.30	26.18
Cr	4.20	4.89
Ti	0.81	0.89

(d)

Figure 3 Microstructural characteristics of a simple aluminide coating on alloy MAR-M 002DS in the heat-treated condition. (a) Backscattered images illustrating the coating microstructure parallel to the surface and along the cross-section. (b) X-ray diffraction pattern derived from the coating surface (β-phase; cubic B2-type superlattice). (c) X-ray energy spectrum representative of the β-phase at the coating surface. (d) Corresponding chemical composition. (e) Identification of α-Cr near the coating surface (dark-field TEM image and corresponding [111] microdiffraction pattern and x-ray energy spectrum). (f) X-ray energy spectrum of the grain boundary Hf-rich phase at the coating surface. (g) Corresponding x-ray wavelength spectrum illustrating the presence of W at grain boundaries. (h) X-ray energy spectrum representative of β-phase in the inner coating layers. (i) X-ray energy spectrum representative of α-phase in the inner coating layers.

Decohesion of Al_2O_3 scale is known to be a relatively common occurrence during cooling or thermal cycling where thermal stresses are developed because of the differences in thermal contraction/expansion coefficients between the scale and substrate [20]. Since the coefficient of thermal expansion of the metallic substrate (bond coat) is typically greater than that of the oxide, compressive stresses are rapidly induced within the oxide making relief by deformation rather difficult and leading to decohesion of the scale [21, 22].

3.2. Microstructure of bond coat in the heat-treated condition

Fig. 3 summarizes the microstructural characteristics of simple aluminide coating on alloy MAR M 002DS in the heat-treated condition. It is observed from Fig. 3a that the coating consists of three distinct layers: i) an outermost fine-grained layer, ii) an intermediate coarse-grained layer, and iii) an inner interdiffusion zone of columnar morphology. These characteristics are typical of an inward aluminide coating produced by inward

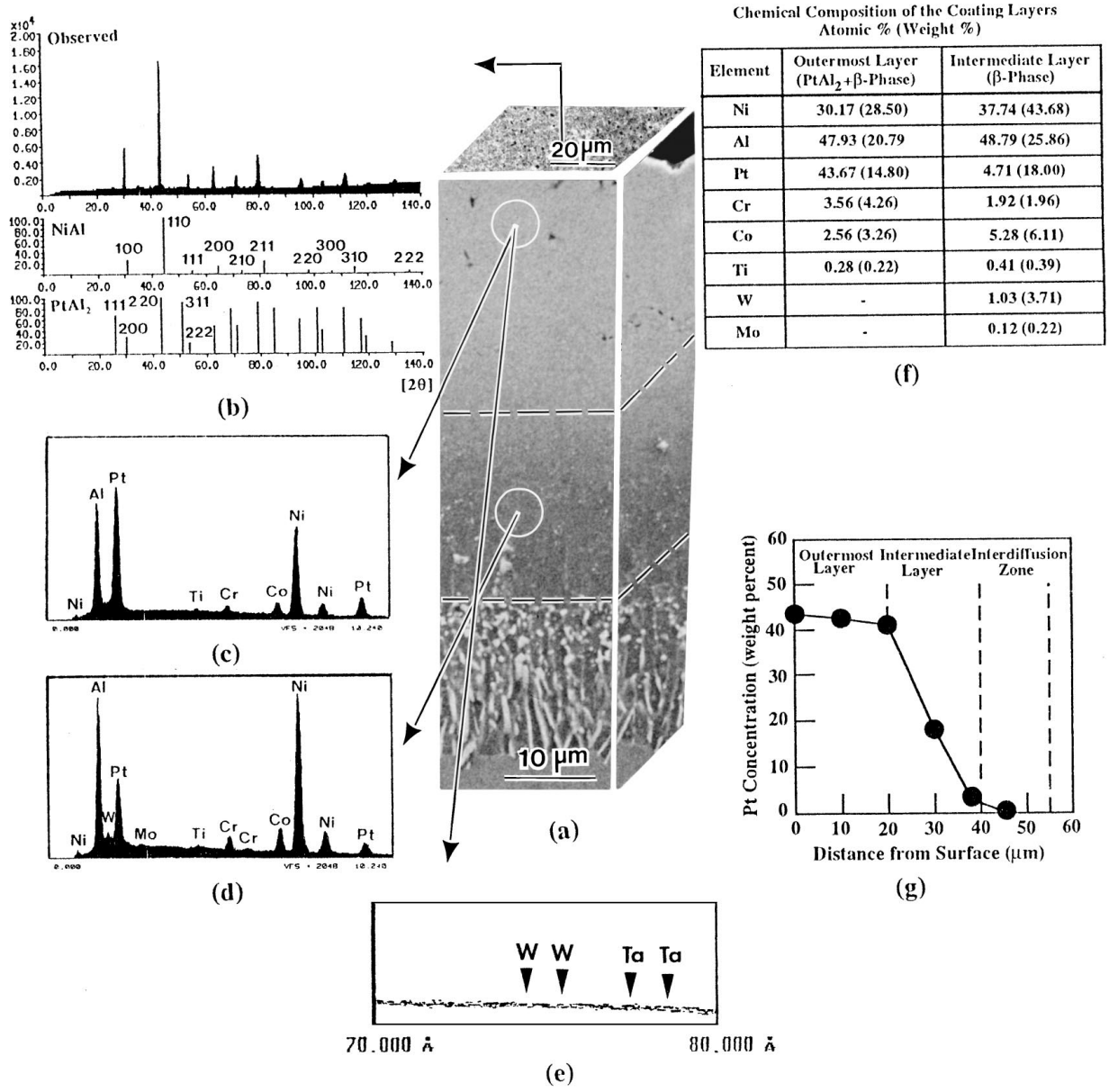

Element	Outermost Layer ($PtAl_2$+β-Phase)	Intermediate Layer (β-Phase)
Ni	30.17 (28.50)	37.74 (43.68)
Al	47.93 (20.79	48.79 (25.86)
Pt	43.67 (14.80)	4.71 (18.00)
Cr	3.56 (4.26)	1.92 (1.96)
Co	2.56 (3.26)	5.28 (6.11)
Ti	0.28 (0.22)	0.41 (0.39)
W	-	1.03 (3.71)
Mo	-	0.12 (0.22)

Figure 4 Microstructural characteristics of a Pt-aluminide coating on alloy MAR-M 002DS in the heat-treated condition. (a) Backscattered images illustrating the coating cicrostructure parallel to the surface and along the cross-section. (b) X-ray diffraction pattern derived from the coating surface; standard patterns of NiAl and $PtAl_2$ are shown. (c) X-ray energy spectrum representative of the outermost coating layer. (d) X-ray energy spectrum representative of the intermediate coating layer. (e) X-ray wavelength spectrum illustrating the absence of W and Ta in the outermost coating layer. (f) Chemical composition of the coating layers. (g) Concentration profile of Pt across the coating layers and into the interdiffusion zone.

diffusion of Al [22, 23]. In this case, substrate elements are transported into the outermost coating layer. As demonstrated in Fig. 3b, the outermost layer consisted of β-NiAl (cubic B2-type superlattice; $a = 0.294$ nm) containing Co,Ti, and some Cr in solid-solution (Fig. 3c and d). Excess Cr and Mo not in solid-solution were precipitated as fine particles of α-Cr,Mo (body-centered cubic; $a = 0.2885$ nm) within the matrix of β-phase as shown in Fig. 1e. Precipitates along grain boundaries at the coating surface (Fig. 3a) were found to be Hf-rich (Fig. 3f) demonstrating the very limited solubility of Hf in the β-phase. Evidently, Hf in the alloy substrate (see Table I) had diffused into the coating during processing. Since very little or no Hf was detected in the inner layers, it appeared that Hf had the tendency to segregate at the coating surface. Also, the precipitate was found to contain a small concentration of W (Fig. 3g). Although the β-phase within the inner layer was found to contain a small concentration of W (Fig. 3h), most of the W was present in the form of (Ni,Co)CrW α-phase precipitates at grain boundaries of the β-phase and within the interdiffusion zone (Fig. 3i). It is possible to conclude from these observations that both Hf and W had limited solubility in the β-phase, however, because of the slow diffusivity of W, it was mostly present within the inner coating layers.

In addition to the W-rich α-phase, the columnar β-phase matrix of the interdiffusion zone was found to contain particles of MC-type carbides (Ta,Ti-rich and Hf-rich). Since these phases are enriched in slow-diffusing refractory transition metals, they could act as effective diffusion barrier between the coating and superalloy substrate improving the coating resistance to oxidation and hot corrosion by restricting loss of Al either by inward diffusion into the substrate and/or outward diffusion of Ni and other substrate elements [24].

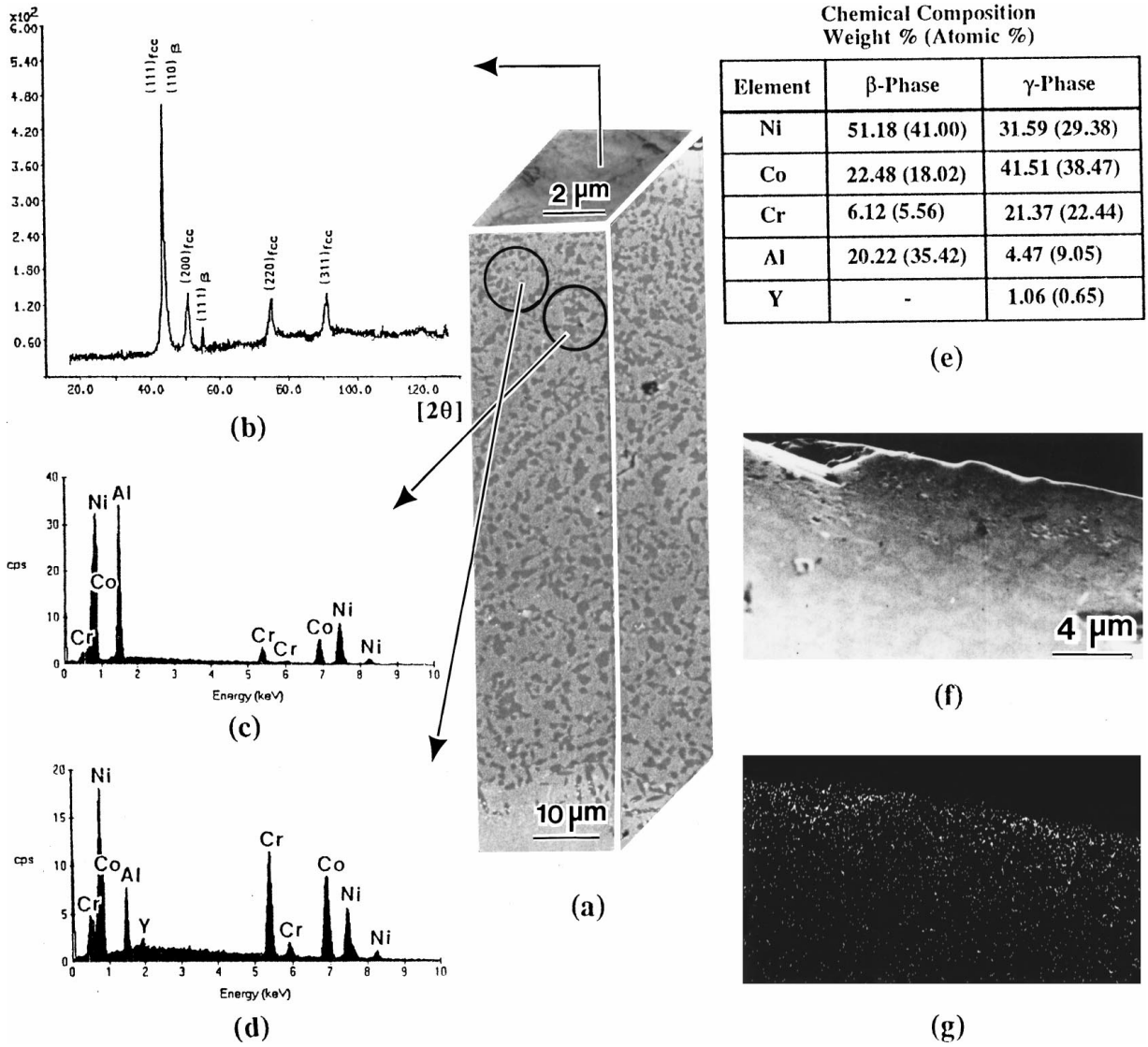

Chemical Composition
Weight % (Atomic %)

Element	β-Phase	γ-Phase
Ni	51.18 (41.00)	31.59 (29.38)
Co	22.48 (18.02)	41.51 (38.47)
Cr	6.12 (5.56)	21.37 (22.44)
Al	20.22 (35.42)	4.47 (9.05)
Y	-	1.06 (0.65)

Figure 5 Microstructural characteristics of an overlay coating [(Ni + Co)CrAlY] on alloy MAR-M 002DS in the heat-treated condition. (a) Backscattered images illustrating the coating microstructure parallel to the surface and along the cross-section. (b) X-ray diffraction pattern derived from the coating surface (c) X-ray energy spectrum representative of the β-phase. (d) X-ray energy spectrum representative of the γ-phase. (e) Chemical composition of the β-phase and γ-phase. (f) Secondary electron image of coating cross-section (SEM mode of an AEM at 200 keV). (g) Corresponding x-ray mapping image of Y.

Differences in superalloy substrate composition were found to be reflected upon the structure and composition of the interdiffusion zone. For example, due to the absence of C in alloy SRR 99 (Table I), its interdiffusion zone contained only W-rich α-phase, and was free of MC-type carbides particularly those enriched in Ta and Ti. Therefore, during subsequent exposure at elevated temperatures, elemental Ta and Ti would be available to diffuse into the coating surface, which could degrade the protective nature of Al_2O_3 scale in contrast with the case of alloy MAR-M 002DS as shown later. In the case of alloy RR2000 (Table I), only Ti would be available to diffuse into the coating. Therefore, the extent of coating degradation by interdiffusion would be expected to vary with superalloy substrate composition through its influence on the structure and composition of the interdiffusion zone.

Among the most important modifications aiming at improving the performance of simple aluminides is the addition of Pt [18]. Similar to a simple aluminide, a Pt-aluminide coating is developed by interaction with the alloy substrate. However, the presence of a Pt-rich phase at the surface could limit the outward diffusion of substrate elements particularly transition metals as well as active elements such as Hf promoting selective oxidation Al resulting in a purer scale of slower growth rate and better adherence [25–28].

Addition of Pt to a simple aluminide results in the formation of a Pt-rich intermetallic phase in the outermost coating layer such as $PtAl_2$, Pt_2Al_3, or PtAl depending upon the coating type [29]. Fig. 4 illustrates the microstructure of a Pt-aluminide coating on alloy MAR M 002DS produced by the addition of Pt to the aluminide coating/substrate system of Fig. 3.

It is observed from Fig. 4a that the coating consisted of two outer layers and an inner interdiffusion zone similar to the case of the above simple aluminide (inward-type coating). However, in comparison with the aluminide coating on the same alloy (Fig. 3), the outermost layer became free of precipitates such as

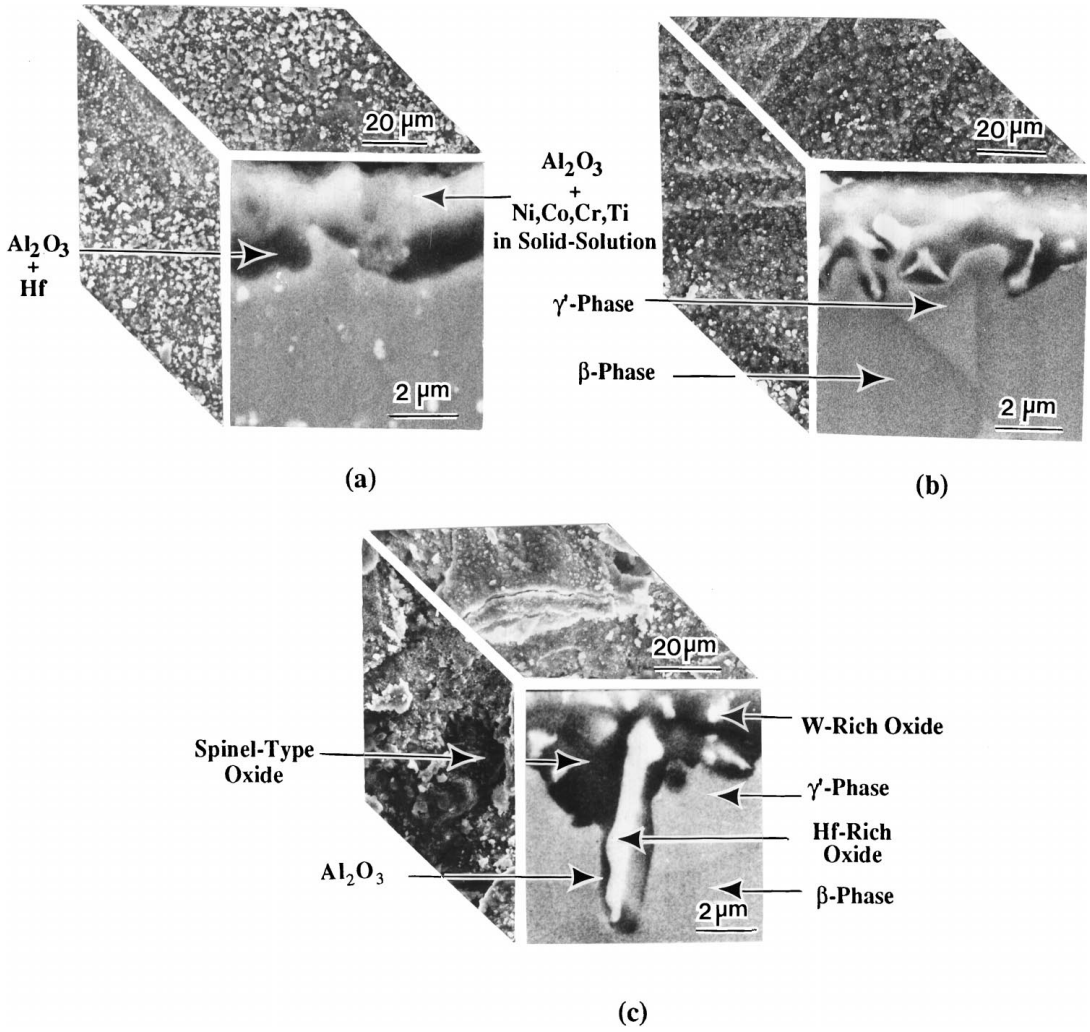

Figure 6 Evolution of the oxide scale developed by a simple aluminide coating on alloy MAR-M 002DS during exposure at 1100 °C. (a) 1 hour of exposure. (b) 24 hours of exposure. (c) 100 hours of exposure.

α-Cr and σ-phase. As shown in Fig. 4b, this layer consisted of a mixture of $PtAl_2$ (cubic; $a = 0.5926$ nm) and β-phase. Also, the outermost layer became free of transition metals (Fig. 4c), however, the intermediate layer was found to contain relatively small concentrations of these elements (Fig. 4d) indicating that Pt had restricted the outward diffusion of these elements during coating formation. Although no Hf was detected in the outermost layer by energy dispersive spectroscopy, its concentration could be very small in contrast with the case of aluminide coating. Small but critical amounts of active elements such as Hf could produce beneficial effects on the protective nature of Al_2O_3 scale, however, larger concentrations could have adverse effects, e.g. [30, 31]. Fig. 4e further confirms the absence of transition metals particularly W and Ta in the outermost coating layer.

Fig. 4f summarizes the chemical composition of the outer coating layers. It could be concluded from this data that the β-phase in the outermost layer contained Pt, which could substitute for Ni. Also, the data indicated that the intermediate layer consisted of β-phase containing Pt. However, as shown in Fig. 4g most of the Pt was concentrated in the outermost layer, and no Pt was present within the interdiffusion zone. A comparison of the microstructural features of the aluminide

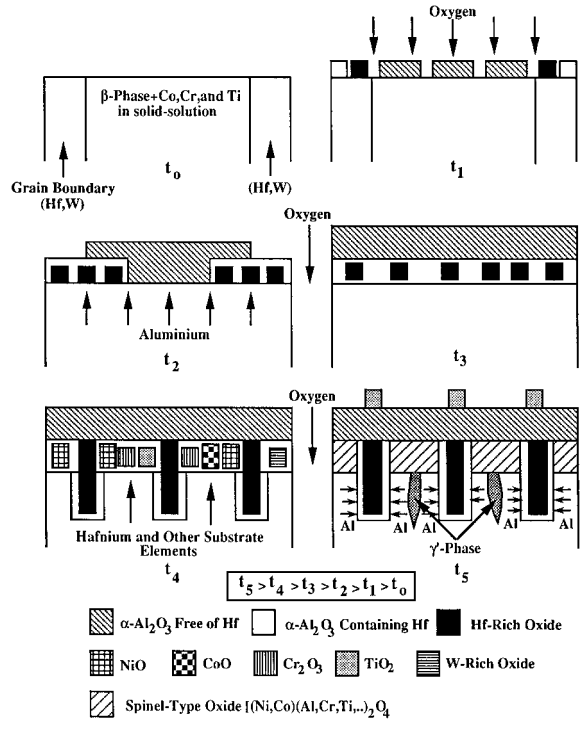

Figure 7 Schematics illustrating the mechanism of oxide formation on a high activity aluminide coating (alloy MAR-M 002DS substrate) as a function of exposure time t at a given temperature.

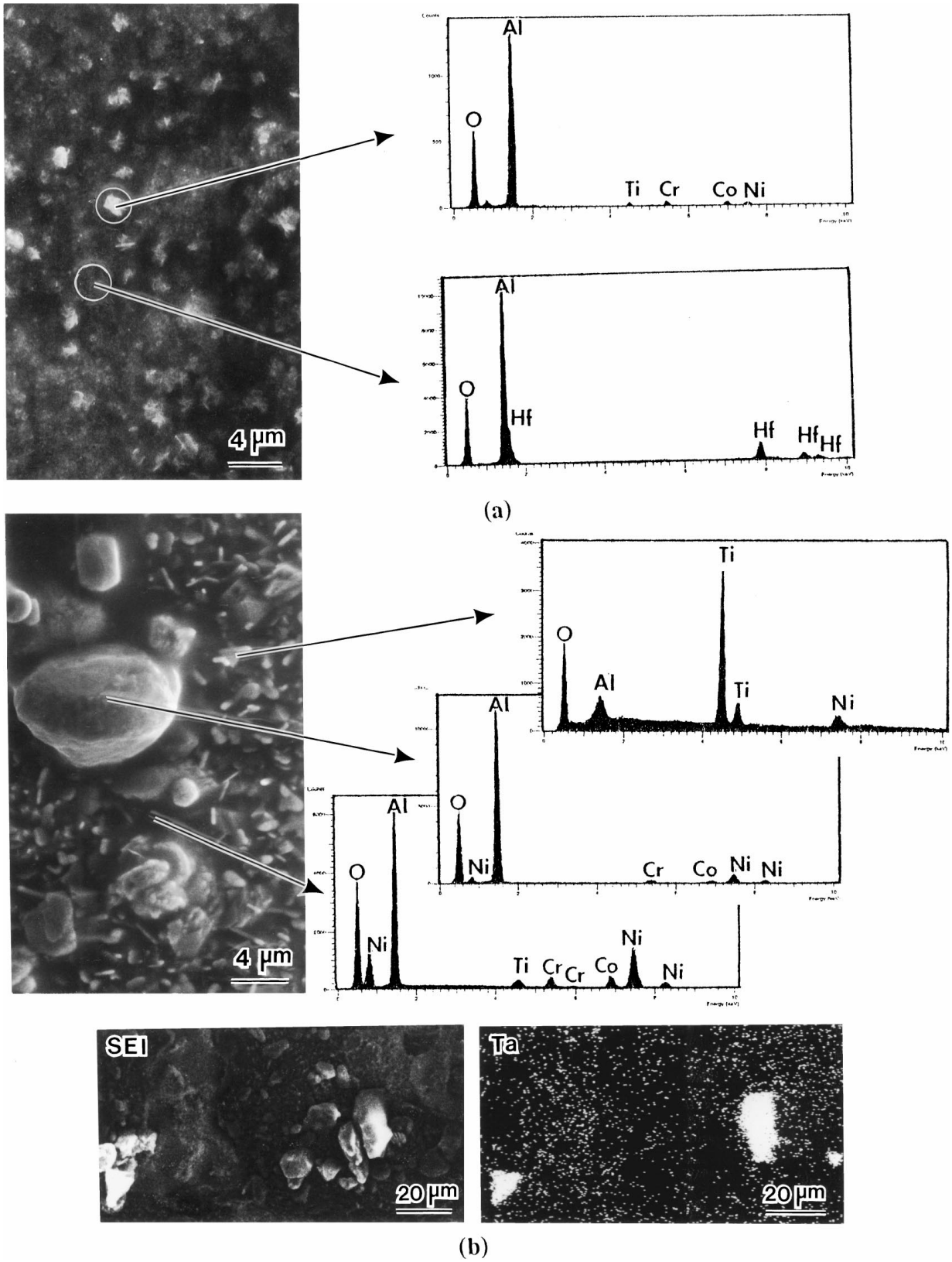

Figure 8 Secondary electron images and corresponding x-ray energy spectra illustrating the morphology and composition of external scale developed by a Pt-aluminide coating on alloys MAR-M 002DS (a) and SRR 99 (b) after 500 hours of exposure at 1100°C in still air.

and Pt-aluminide coatings on the same alloy in the heat-treated condition (Figs 3 and 4) revealed that the addition of Pt to the aluminide coating had increased its diffusional stability, which could promote selective oxidation of Al as shown later.

Fig. 5 illustrates typical microstructural features of an MCrAlY coating on alloy MAR M 002DS in the heat-treated condition. As shown in Fig. 5a and b, the coating consisted of β-phase (B2-type superlattice; $a = 0.289$ nm) dispersed in a matrix of γ-phase (face-centered cubic solid-solution; $a = 0.358$ nm). Yttrium was found to be partitioned to the γ-phase consistent with its known limited solubility in the β-phase as shown in Fig. 5c and d. As shown in the data of

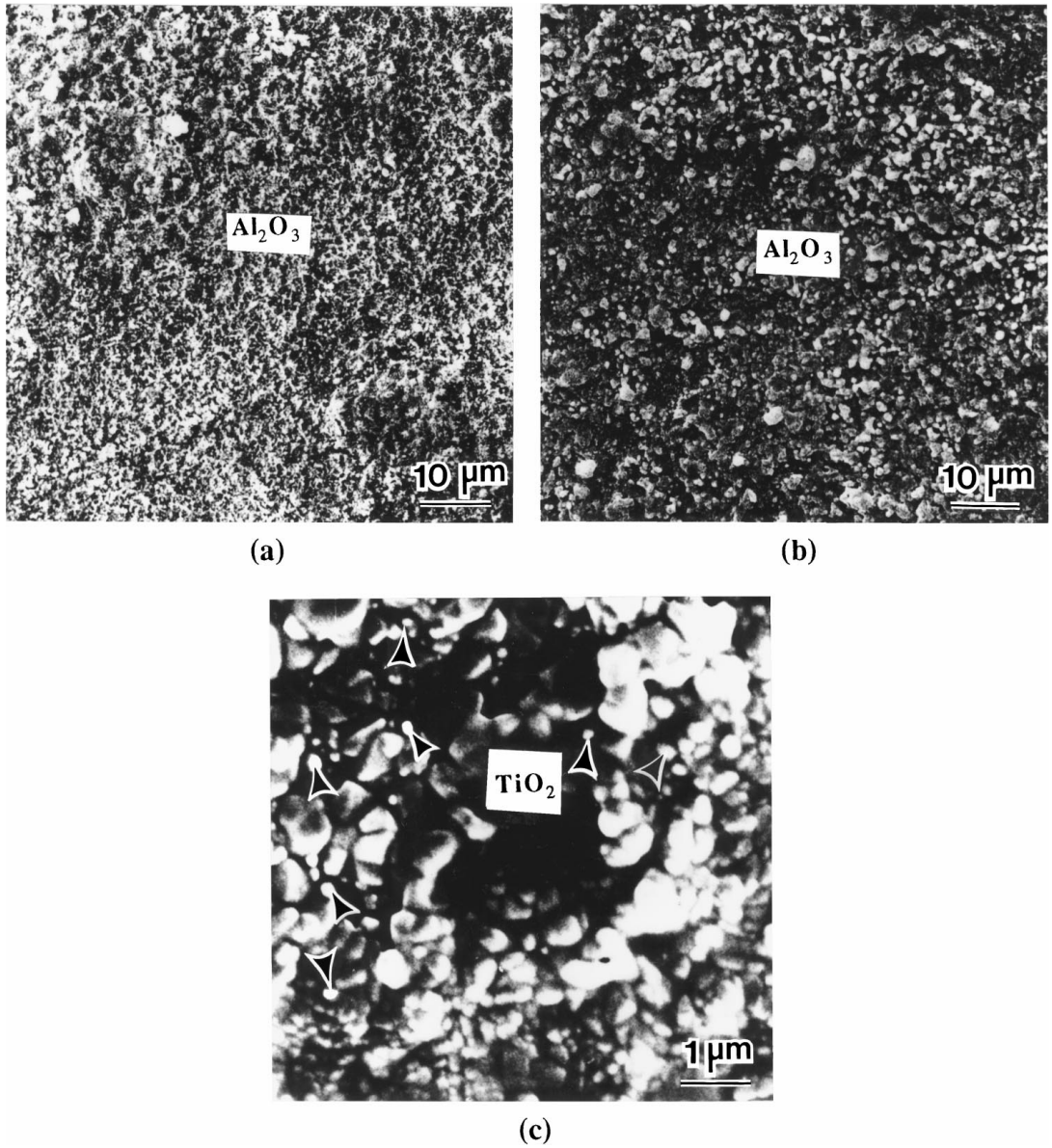

Figure 9 Secondary electron images illustrating the scale developed by an overlay coating [(Ni + Co)CrAlY] after 24 hours of exposure at 1100 °C. (a) Alloy MAR-M 002DS substrate. (b), (c) Alloy RR 2000 substrate; particles of Ti-rich oxide are indicated by the arrows in (c).

Fig. 5e, the β-phase was Ni-rich and the γ-phase was Co-rich. Although some of the Y was found at the coating-substrate interface in the form of a Ni-Y phase, elemental Y in the γ-phase exhibited a tendency to segregate near the coating surface as demonstrated in Fig. 5f and g. In contrast with diffusion aluminide coatings (Figs 3 and 4), the outermost coating layer was essentially free of substrate elements reflecting the very little or no interaction with the alloy substrate during coating formation. This could contribute at least partially to longer life of the respective thermal barrier coating system as observed in Fig. 2.

As demonstrated below, the characteristic microstructural features of various types of coatings in the heat-treated condition were reflected upon their oxidation behavior at elevated temperatures.

3.3. Oxidation behavior

Fig. 6 illustrates the evolution of oxide scale developed by the aluminide coating on alloy MAR-M 002DS during exposure at 1100 °C. During the early stages of exposure (Fig. 6a), the coating developed two layers of Al_2O_3: i) an outer layer containing small concentrations of Cr, Ti, Co, and Ni, and ii) an inner layer containing Hf and/or fine Hf-rich oxide particles improving its protective nature. One possible mechanism is retarding crack propagation through the scale [32]. Another mechanism is blocking lattice diffusion through the scale reducing its growth rate [33]. Also, it is possible that Hf segregates to grain boundaries of Al_2O_3 maintaining a fine-grained scale of improved mechanical strength similar to the case of Y in overlay coatings as demonstrated later.

With continued exposure, relatively large Hf-rich oxide particles penetrating the coating were observed (Fig. 6b). Coincident with this behavior was the partial transformation of β-phase into γ'-phase (Ni_3Al composition) along the grain boundaries as shown in Fig. 6b. It is observed that the Hf-rich oxide particles were exclusively present in the vicinity of coating regions transformed into the γ'-phase (Fig. 6b and c). Since Hf is

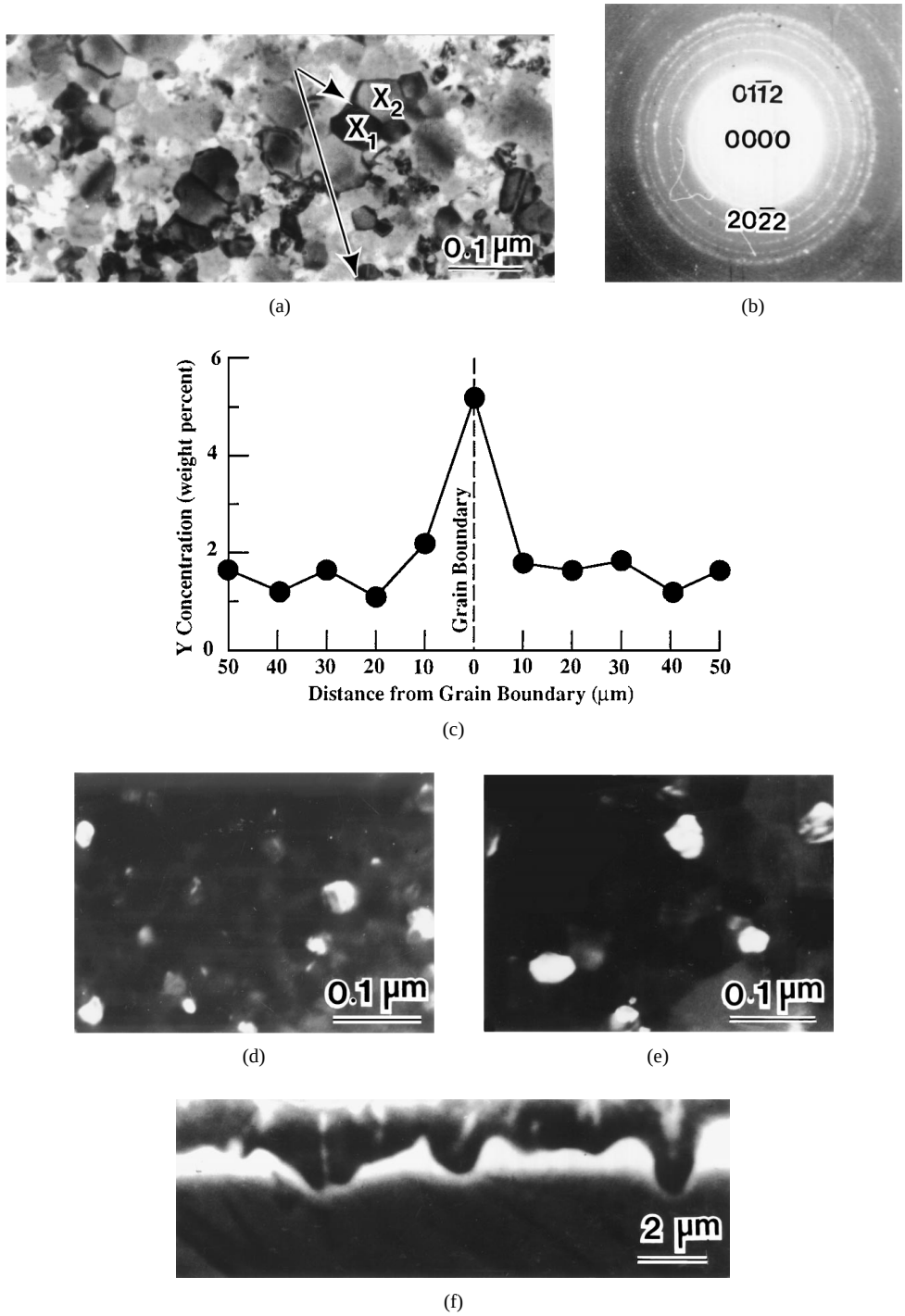

Figure 10 Role of Y i n an overlay coating [(Ni + Co)CrAlY] on alloy MAR-M 002DS. (a) Bright-field TEM image illustrating the grain structure of Al_2O_3 scale parallel to the plane of oxidation after 24 hours of exposure at 1000°C. (b) Corresponding selected-area diffraction pattern indexed in terms of α-Al_2O_3 structure. (c) Concentration profile of Y across a grain boundary. (d) and (e) are dark-field TEM images illustrating the grain size of the scale after 24 hours and 1000 hours of exposure at 1000°C respectively. (f) Secondary electron image illustrating Y-rich oxide pegs penetrating the coating (100 hours of exposure at 1100 °C).

known to have high solubility in the γ'-phase, the above observations indicated that the β-phase $\rightarrow$ γ'-phase transformation could have been initiated within the pre-existing Hf-rich phase at the grain boundaries (see Fig. 3). Further oxidation caused the Hf-rich oxide particles to grow into relatively large pegs enveloped by Al_2O_3 as shown in Fig. 6c. Associated with this behavior was the development of less protective spinel-type oxide near the coating surface as well as spallation of the external scale. Based upon these observations, it is possible to summarize the oxidation mechanism as follows.

It is well known that Al_2O_3 and HfO_2 are among the most stable oxides as indicated by their enthalpy of formation [34]. Also, it is known that active elements, e.g. Hf, increase the Al activity [35]. Therefore it would be expected that as the Hf-rich oxide continued to grow inward, it drew Al into the stable HfO_2/Al_2O_3 assembly depleting the coating in Al. Simultaneously, the presence of larger concentration of W in the alloy could restrict the outward diffusion of Al as discussed earlier. Eventually, the coating became depleted in Al promoting the transformation of β-phase into the Ni-rich

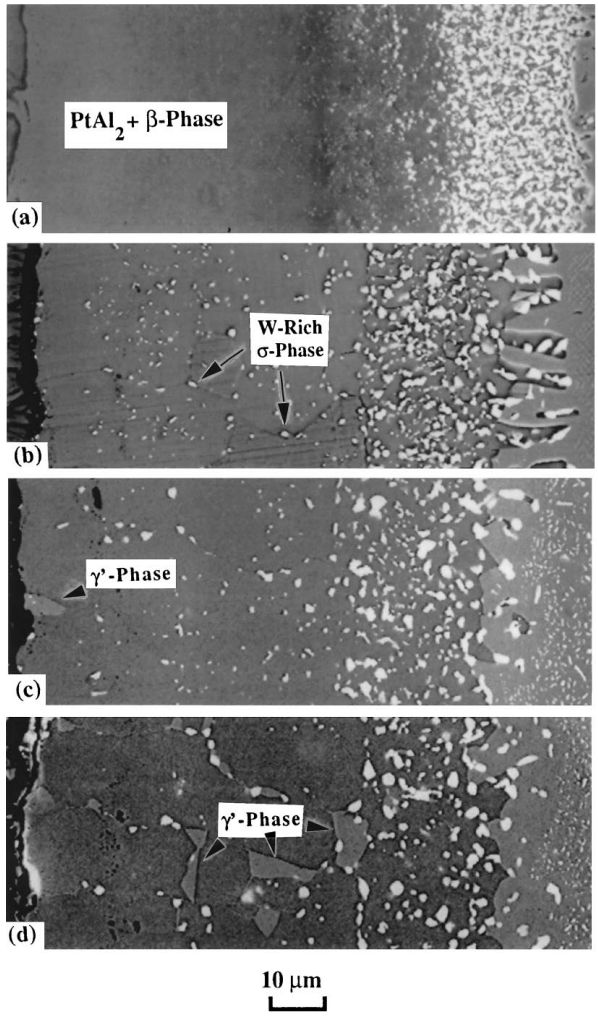

Figure 11 Backscattered electron images illustrating the effect of exposure time at 1150 °C on the microstructure of Pt aluminide bond coat. (a) Unexposed. (b) 24 hours of exposure. (c) 48 hours of exposure. (d) 72 hours of exposure (alloy SRR99 substrate).

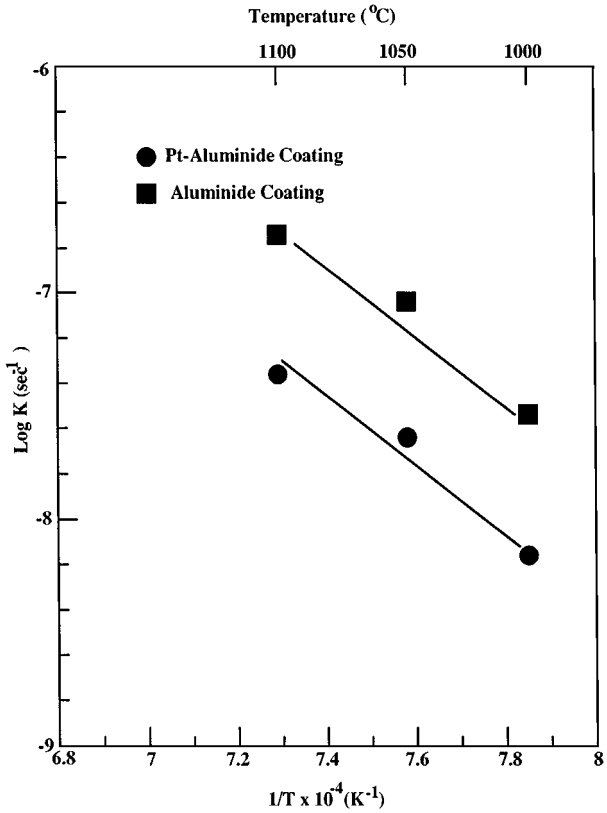

Figure 12 Comparative temperature-dependent reaction rate constant (K) for interdiffusion between aluminde and Pt-aluminide coatings on the same superalloy substrate as determined from the growth of interdiffusion zone.

γ'-phase (Ni_3Al) as well as the formation of less protective oxides by outward diffusion of substrate elements. Schematics illustrating these processes for a high activity aluminide coating on alloy MAR-M 002DS are shown in Fig. 7. Also, the adhesion of Al_2O_3 scale developed by a Pt-aluminide coating could be degraded by the same mechanism shown in Fig. 7, however, a longer exposure time at a given temperature would be required to develop a given oxide morphology. It is to be noted that the exact oxidation mechanism is modified by the respective superalloy substrate composition as illustrated in the example given below.

Fig. 8 illustrates the components of external scale developed by the same Pt-aluminide coating on alloys MAR-M 002DS and SRR 99 after 500 hours of exposure at 1100 °C. It is observed from Fig. 8a that the external scale of alloy MAR-M 002DS contained only Al_2O_3 similar to the case of a simple aluminide (Fig. 6), however, the external scale of alloy SRR 99 (Fig. 5b) contained a high density of fine Ti-rich particles identified as TiO_2 as well as a Ta-rich oxide. Earlier studies showed that Ti could have adverse effects on oxidation resistance by forming TiO_2 particles degrading the adherence of Al_2O_3 scale [36, 37]. In the case of Ta, there are some discrepancies regarding adverse effects particularly at high concentrations [38, 39]. It is then evident that the coating on alloy MAR-M 00R is more resistant to oxidation in comparison with alloy SRR 99. Similar to the case of diffusion aluminide coatings, the oxidation behavior of overlay coatings was found to be a function of superalloy substrate composition as demonstrated below.

Fig. 9 shows the microstructural features of the external scale developed by the overlay coating on alloys MAR M 002DS and RR2000 at 1100 °C. After 24 hours of exposure, the external scale developed by the coating on alloy MAR-M 002DS was observed to be more compact and have a finer structure (Fig. 9a) in comparison with the case of alloy RR 2000 (Fig. 9b). Although the scale of alloy MAR-M 002DS was found to consist of only Al_2O_3, the scale of alloy RR 2000 contained particles of TiO_2 as shown in Fig. 9c. As indicated above, TiO_2 particles could degrade the adherence of Al_2O_3 scale.

In general, no Y was detected in within the external scale developed by MCrAlY coatings at least within the detection limits of energy dispersive x-ray spectroscopy (about 0.2 weight %). However, Y was detected within the inner layers of the scale particularly near the oxide-bond coat interface as summarized in Fig. 10 indicating that Y could modify the oxidation behavior by more than one mechanism. Fig. 10a shows a typical grain structure of Al_2O_3 scale near the oxide-bond coat interface and parallel to the plane of oxidation. A corresponding selected-area diffraction pattern indexed in terms of the structure of α-Al_2O_3 is shown in Fig. 10b.

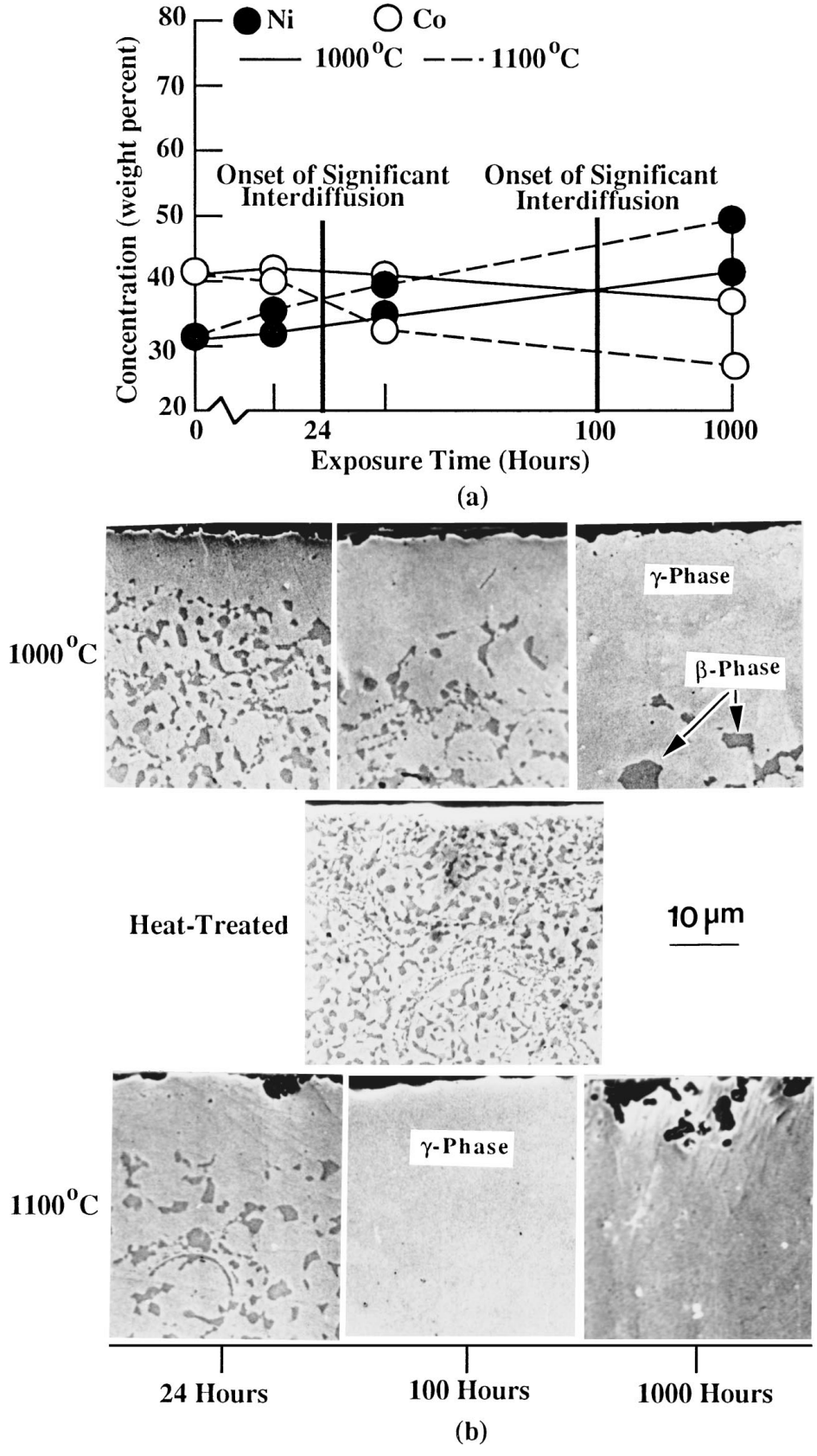

Figure 13 Thermal stability characteristics of an overlay coating on alloy MAR-M 002DS at 1000 °C and 1100 °C. (a) Effect of exposure time on the concentrations of Ni and Co in the γ-phase. (b) Effect of exposure time on the coating morphology.

It is observed from Fig. 10c that Y had a tendency to segregate at grain boundaries of Al_2O_3. This segregation could stabilize a fine-grained structure as shown in Fig. 10d and e improving the high-temperature mechanical strength of the scale [35, 40, 41] as well as reducing its growth rate and in turn the extent of growth stresses [35, 42]. Another beneficial effect of Y segregation to grain boundaries could be filing of voids or pores along grain boundaries and thus improving the scale cohesion [43, 44]. A relatively small concentration of Y in solid-solution as observed in Fig. 10c could decelerate the kinetics of Al lattice diffusion further contributing

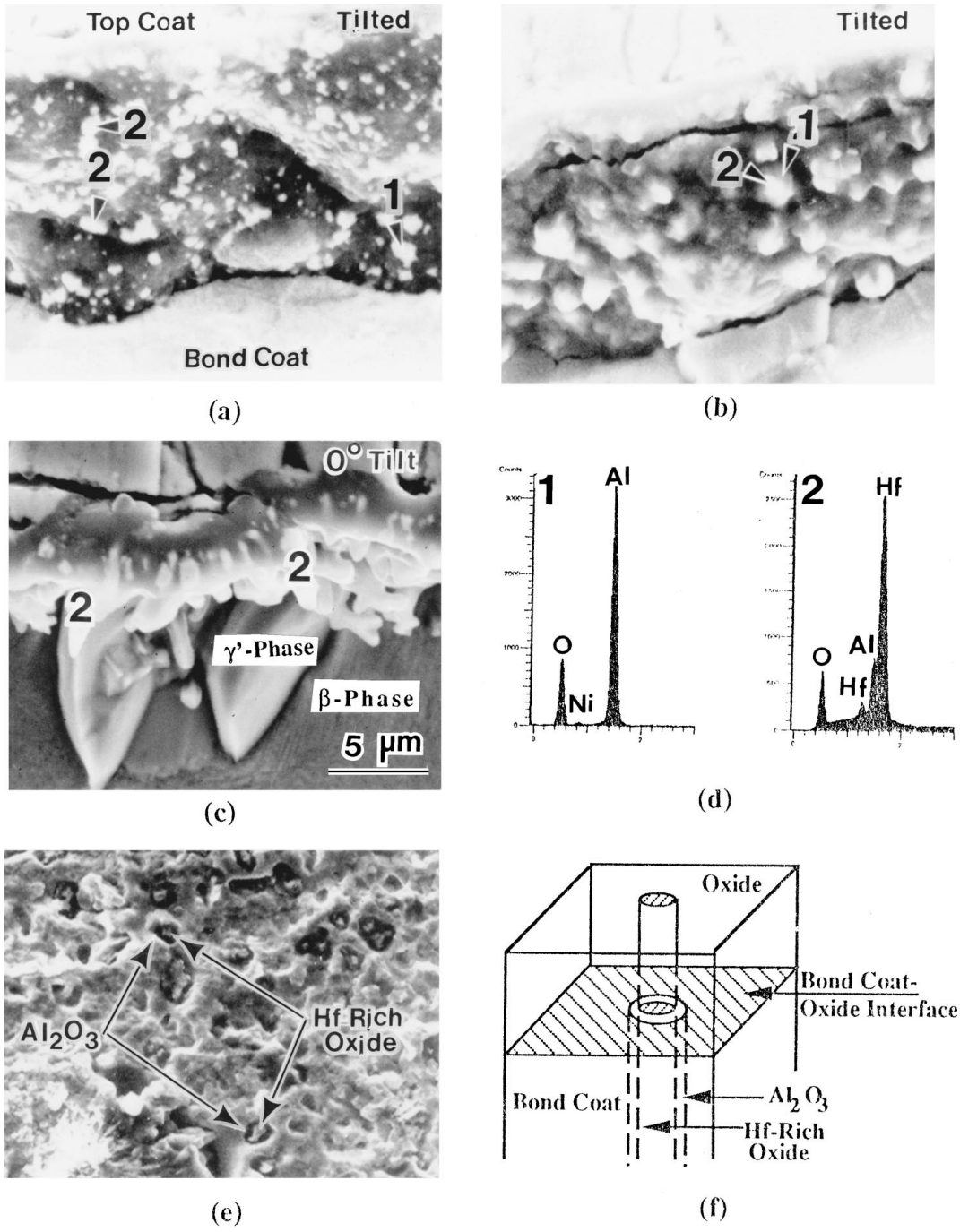

Figure 14 Failure mode of a TBC system on alloy MAR-M 002DS at 1150°C (Pt-aluminide bond coat). (a) and (b) are secondary electron images illustrating the interfacial oxide morphology after 24 hours and 48 hours of exposure respectively. (c) Secondary electron image illustrating the formation of γ'-phase in the outermost layer of bond coat after 48 hours of exposure. (d) X-ray energy spectra illustrating the composition of oxide scale corresponding to regions 1 and 2 in (a), (b), and (c). (e) Secondary electron image illustrating the morphology of bond coat surface exposed by failure after 96 hours of exposure. (f) A schematic illustration of the oxide morphology leading to decohesion between the oxide and bond coat.

to a reduced scale growth rate [45–47]. Yttrium could also improve the protective nature of Al_2O_3 by forming Y-rich oxide pegs as shown in Fig. 10f pinning the scale to the substrate [48]. Other possible mechanisms are based upon the role of Y as a S-getter improving the scale adherence [49, 50], and as a strengthener of the oxide-substrate interface [51].

3.4. Coating degradation modes: Thermal stability characteristics

Earlier work suggests that loss of Al by diffusion into the substrate eventually leading to a relatively homogeneous alloy is the principal degradation mode of aluminide coatings [24]. In the case of aluminide coatings on Ni-base alloys, however, it has been argued that the principal degradation mode is loss of Al due to continued oxide formation and spallation [23]. Although this model may be valid at temperatures less than about 1050 °C, other studies indicate that the coating is first depleted in Al by interdiffusion with the substrate followed by rapid degradation due to formation of oxides less protective than Al_2O_3 [30]. However, both the oxidation resistance and thermal stability of the coating can be sensitive function of its manufacturing history and alloy substrate composition. For example, in

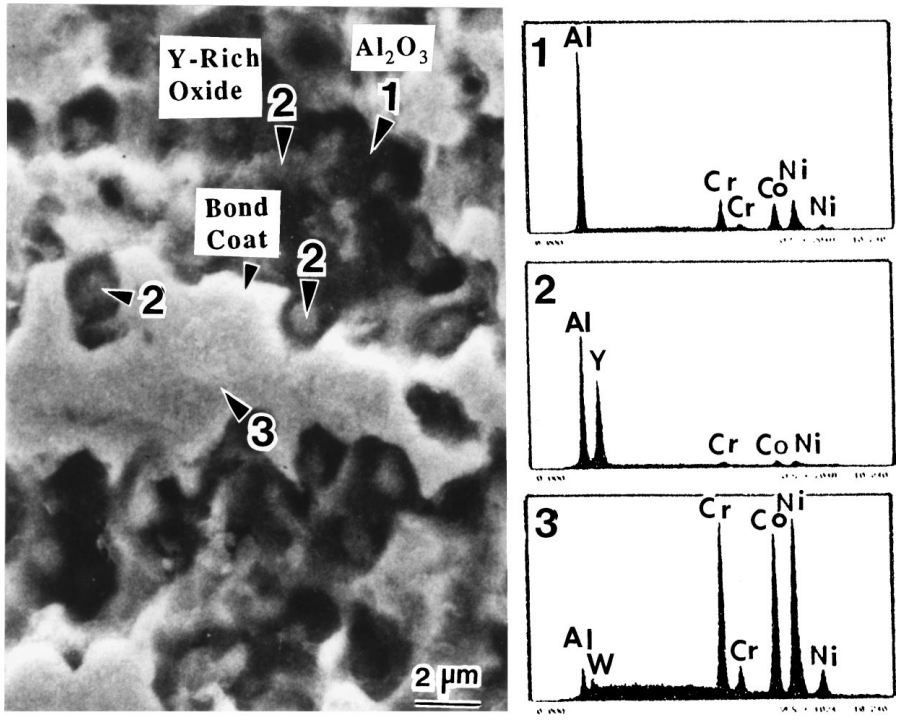

Figure 15 Backscattered electron image and corresponding energy dispersive x-ray spectra illustrating the elemental compositions of various regions marked 1, 2, and 3 of MCrAlY bond coat surface exposed by failure of the TBC system at 1150°C (alloy MAR M 002DS substrate).

the case of an inward diffusion aluminide coating (see Fig. 3), the outermost layer was found to contain all substrate elements leading to precipitation of α-Cr reducing the thermal stability of β-phase and promoting its transformation into the Ni-rich γ'-phase [24]. Also, the presence of Ti in the outermost coating layer, e.g. alloy SRR99 and to a larger extent in the case of alloy RR2000, could degrade the adherence of Al_2O_3 scale as pointed out earlier.

Our studies showed that both the simple aluminides and Pt-aluminides were degraded by the same mechanism involving oxidation and interdiffusion at temperatures $\geq$1000 °C. For example, Fig. 11 shows the effect of exposure time at 1150 °C on the microstructure of Pt-aluminide coating on alloy SRR99. After 24 hours of exposure, the grain boundaries of β-phase were delineated by W-rich σ-phase particles as shown by comparing Fig. 11a and b. Also, the structure of the interdiffusion zone became coarser relative to the unexposed condition indicating the onset of significant interdiffusion. Partial transformation of the β-phase into γ'-phase was observed after 48 hours of exposure as illustrated in Fig. 11c. With continued exposure (Fig. 11d), the density of the γ'-phase was increased, and the σ-phase particles became coarser. However, as determined from the growth of interdiffusion zone for a given superalloy substrate, the Pt-aluminide coating exhibited a slower degradation rate in comparison with simple aluminides as shown in Fig. 12. This reflected the greater diffusional stability of the Pt-aluminide coating in comparison with the aluminide coating consistent with their initial microstructural characteristics (see Figs 3 and 4).

Similar to aluminide coatings, overlay coatings were found to be degraded by oxidation and interdiffusion at temperatures $\geq$1000 °C. Earlier studies showed that the onset of significant interdiffusion is indicated by about equal proportions of Ni and Co in the initially Co-rich γ-phase [24]. For example, Fig. 13a illustrates the effect of exposure time at 1000 °C and 1100 °C on the concentrations of Ni and Co in the γ-phase and the corresponding effect on coating morphology is shown in Fig. 13b. As expected, the kinetics of interdiffusion were accelerated as the temperature was raised from 1000 °C to 1100 °C. With continued exposure, a β-phase depleted zone was developed at the coating surface and it increased in width with time as the coating became depleted in Al by the combined effects of oxidation and interdiffusion. Simultaneously, the β-phase in the inner coating layers became rather blocky, and eventually the entire coating layer was transformed into γ-phase (Ni-rich solid-solution).

3.5. Failure mechanism of thermal barrier coating systems

Thermal barrier coating systems using either a diffusion aluminide or an overlay as a bond coat were found to fail by void formation and coalescence near the oxide-bond coat interface. However, the exact behavior varied from one alloy substrate to another.

To exemplify the behavior of diffusion aluminide bond coats, Fig. 14 summarizes the sequence of events leading to failure of the coating system on alloy MAR-M 002DS at 1150 °C. During the earlier stage of exposure, Hf-rich oxide particles were formed beneath the thermally grown layer of Al_2O_3 (Fig. 14a). With continued exposure, the oxide particles grew into relatively coarse pegs penetrating the bond coat (Fig. 14b). Corresponding to this behavior, the β-phase was partially transformed into the Ni-rich γ'-phase (Fig. 14c). This could be related at least partially to the tendency of

Hf-rich oxide pegs to be enveloped by Al_2O_3 (Fig. 11c and d) causing localized depletion in Al as discussed earlier. Voids observed at the bond coat surface exposed by failure contained Hf-rich oxide particles enveloped by Al_2O_3 as shown in Fig. 14e. These observations suggested that internal oxidation of Hf diffusing from the alloy substrate as schematically illustrated in Fig. 14f had eventually led to localized high levels of stress concentration, which could only be accommodated by forming voids. A similar behavior was observed in the case of MCrAlY overlay coating as illustrated in Fig. 15. However, in this case, the failure was promoted by internal oxidation of Y in the coating. In the case of single-crystal alloys free of Hf, oxidation of Ti near the oxide-bond coat interface played a more dominant role in causing decohesion of the scale by void formation.

It could be concluded from the above results that although active elements such as Hf and Y could significantly improve the protective nature of the interfacial oxide layer between the top coat and bond coat, it is very important to be able to control the concentration of active elements present near the interface. This may be achieved by combining Pt and active elements in bond coats of better thermal stability than the conventional Pt aluminides.

4. Conclusions

For a given alloy substrate, overlay bond coats were found to provide the best performance in thermal barrier coating systems followed by platinum aluminides and simple aluminides. However, all types of bond coats were degraded by interdiffusion and oxidation, and the coating system failed by the same mechanism involving decohesion of the oxide at the oxide-bond coat interface. This could be related to outward diffusion of substrate elements forming non-protective oxide scale near the bond coat surface. Incorporation of platinum as well as controlled amounts of active elements into the bond coats could improve their performance.

Acknowledgements

It is a pleasure to acknowledge the financial support of Rolls-Royce plc who also provided the material used in this study. Also, the support of the Research Institute of King Fahd University of Petroleum and Minerals where the characterization study was carried out is greatly appreciated.

References

1. G. L. WILDE, *J. Aerospace Eng.* **209**(G2) (1995) 85.
2. C. T. SIMS, *Advanced Materials and Processes* **139**(6) (1991) 32.
3. G. W. MEETHAM, *High Temp. Mater.* **13A** (1990) 25.
4. H. LAMMERMAM and G. KIENEL, *Advanced Mater. Process.* **140**(6) (1991) 18.
5. J. H. WOOD and E. H. GOLDMAN, in C. T. Sims, N. S. Stoloff and W. C. Hagel (eds.), Wiley, New York, 1987, p. 359.
6. J. R. NICHOLLS and D. J. STEPHENSON, *Met. and Mater.* **7** (1991) 156.
7. T. N. RHYS-JONES and F. C. TORIZ, *High Temp. Tech.* **7** (1989) 161.
8. A. BENNETT, F. C. TORIZ and A. B. THAKKER, *Surface and Coatings Tech.* **23** (1987) 359.
9. H. M. TAWANCY, N. SRIDHAR, N. M. ABBAS and D. RICKERBY, *J. Mater. Sci.* **33** (1998) 681.
10. U. DIETL, *Surface and Coatings Tech.* **68/69** (1994) 17.
11. J. H. SUN, E. CHANG, C. H. CHAO and M. J. CHENG, *Oxid. Met.* **40**(5/6) (1993) 465.
12. S. M. MEIER, D. M. NISSLEY, K. D. SHEFFLER and T. A. CRUSE, *Trans. ASME* **114** (1992) 258.
13. W. LIH, E. CHANG, B. C. WU and C. H. CHAO, *Oxid. Met.* **36**(3/4) (1991) 221.
14. B. C. WU, C. H. CHAO and E. CHANG, *Mater. Sci. Eng.* **A124** (1990) 215.
15. B. C. WU, E. CHANG, C. H. CHAO and M. L. TASI, *J. Mater. Sci.* **25** (1990) 1112.
16. R. A. MILLER, *J. Eng. Gas Turbines and Power* **111** (1989) 301.
17. G. W. GOWARD and L. W. CANNON, *Trans. of ASME* **110**(1) (1988) 150.
18. J. S. SMITH and D. H. BOONE, Gas Turbine and Aeroengine Congress and Exposition, Brussels, Belgium, June 1990, ASME Paper No. 90-GT-319.
19. H. HERMAN, *Advanced Materials and Processes* **137** (1990) 41.
20. F. H. STOTT, in "The role of Active Elements in the Oxidation Behavior of High Temperature Metals and Alloys," edited by E. Lang (Elsevier Applied Science, London, 1989) p. 3.
21. J. E. HARRIS, *J. Met.* **39**(1) (1987) 34.
22. G. W. GOWARD and D. H. BOONE, *Oxid. Met.* **3**(5) (1971) 475.
23. G. W. GOWARD, *J. Met.* **22**(10) (1970) 31.
24. P. TOMASZEWICZ and G. R. WALLWORK, in "Reviews of High Temperature Materials," edited by J. Newkirk (Freund Publishing House, London, 1982) p. 49.
25. H. M. TAWANCY, N. SRIDHAR, N. M. ABBAS and D. RICKERBY, *Scripta Met. et Materialia* **33**(9) (1995) 1431.
26. H. M. TAWANCY, N. M. ABBAS and T. N. RHYS-JONES, *Surface and Coatings Tech.* **49** (1991) 1.
27. J. SCHAFFER, G. M. KIM, G. H. MEIER and F. S. PETTIT, in "The Role of Active Elements in the Oxidation Behavior of High Temperature Metals and Alloys," edited by E. Lang (Elsevier Applied Science, London, 1989) p. 231.
28. M. R. JACKSON and J. R. RAIRDEN, *Met. Trans.* **8A** (1977) 1697.
29. R. STREIFF and D. H. BOONE, *J. Mater. Eng.* **10**(1) (1988) 15.
30. H. M. TAWANCY, N. SRIDHAR, N. M. ABBAS and D. RICKERBY, *Scripta Met. et Materialia* **33**(9) (1995) 1431.
31. D. DELAUNAY and A. M. HUNTZ, *J. Mater. Sci.* **17** (1982) 207.
32. K. T. FABER and A. G. EVANS, *Acta Met.* **31** (1983) 565, 577.
33. C. S. GIGGINS and F. S. PETTIT, *Met. Trans.* **2** (1971) 1071.
34. A. W. SEARCY, "Chemical and Mechanical Behavior of Inorganic Materials," edited by A. W. Searcy, D. V. Ragone and U. Colombo (Wiley Interscience, New York, 1970) p. 33.
35. A. M. HUNTZ, in "The Role of Active Elements in the Oxidation Behavior of High Temperature Metals and Alloys," edited by E. Lang (Elsevier Applied Science London, 1989) p. 81.
36. A. BOUMAZA, G. MOULIN and A. M. HUNTZ, *Oxid. Met.* **30**(3/4) (1988) 141.
37. M. H. LAGRANGE, A. M. HUNTZ and J. H. DAVIDSON, *Corrosion Sci.* **24**(7) (1984) 613.
38. M. LEVY, P. FARRELL and F. S. PETTIT, *Corrosion NACE,* **42**(12) (1986) 708.
39. C. A. BARRETT, R. V. MINER and D. R. HULL, *Oxid. Met.* **20**(5/6) (1983) 255.
40. H. HINDAM and D. P. WHITTLE, *ibid.* **18**(5/6) (1982) 245.
41. P. KOFSTAD, in "The Role of Active Elements in the Oxidation Behavior of High Temperature Metals and Alloys," edited by E. Lang (Elsevier Applied Science, London, 1989) p. 367.
42. J. JEDLINSKI, *ibid.* (1989) p. 131.
43. J. R. NICHOLLS and P. HANCOCK, *ibid.* (1989) p. 195.
44. T. A. RAMANARAYANAN, M. RAGHAVAN and R. PETKOVIC-LUTON, *Oxid. Met.* **22**(3/4) (1984) 83.

45. *Idem., J. Electrochem. Soc.* **131** (1984) 923.
46. K. P. R. REEDY, J. L. SMIALEK and R. A. COPPER, *Oxid. Met.* **17**(5/6) (1982) 429.
47. F. A. GOLIGHTLY, F. H. STOTT and G. C. WOOD, *ibid.* **10** (1976) 163.
48. B. LUSTMAN, *Trans. TMS-AIME* **188** (1950) 995.
49. J. G. SMEGGIL, in "The Role of Active Elements in the Oxidation Behavior of High Temperature Metals and Alloys," edited by E. Lang (Elsevier Applied Science, London, 1989) p. 271.
50. J. L. SMIALEK, *Metall. Trans.* **18A** (1987) 164.
51. K. L. LUTHRA and C. L. BRIANT, *Oxid. Met.* **26** (1986) 397.

Received 25 February
and accepted 16 August 1999